ELTac: A vision-based electroluminescent tactile sensing skin for force localization and magnitude estimation

Lanhui Fu, Dip K. Saha, Shivraj Shere, Yanan Li, *Senior Member, IEEE*, Hareesh Godaba, *Member, IEEE*

***Abstract*— Large area tactile sensing for robotic manipulators is an important capability to enable robots to perceive interactions with environment around them and for intuitive human-robot collaboration. In this paper, we introduce a novel vision-based tactile sensing methodology that employs electroluminescent panels with a deformable soft skin that modulates light intensity based on applied forces to realize force localization and magnitude estimation for multi-point contact scenarios. The tactile sensing module is composed of a transparent rigid skeleton, a sensing skin composed of a thin and flexible electroluminescent panel, a deformable translucent elastomer layer with a pyramid pattern and an opaque outer layer. When a force is applied onto the skin, the deformable layer deforms modulating the intensity of light passing through the transparent layer which is detected by a camera embedded inside the module. We utilize image processing, camera models and statistical fitting to localize single and multiple touch points as well as estimate the magnitude of the forces applied. Finally, the proposed algorithm is tested with five different indenters, and the localization error and the intensity-force mapping are analyzed. A localization accuracy of 6.63mm has been achieved and normal forces from 3.1N to 9.4N can be detected with an accuracy of 9.3-11.7% error range. This work provides a simple and effective solution for the acquisition of position and force magnitude information in human-robot interaction tasks such as guidance and demonstration.**

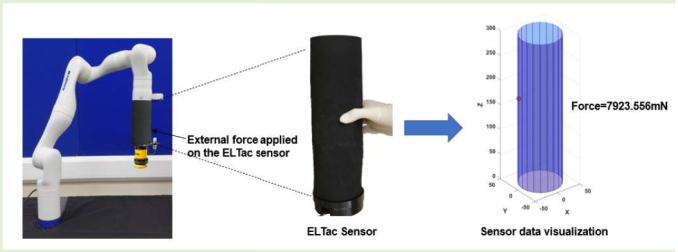

***Index Terms*— Tactile sensing, vision-based, force localization, force magnitude**

I. Introduction

With the growth of robots in the fields of medical treatment, nursing, and industrial processing, the demand for interaction between humans and robots is increasing. Robots are expected to have perception capabilities such as vision and touch to enable versatile interactions with humans. In recent years, although visual sensing has enabled robots with observation capabilities similar to human eyes [1], the acquisition of physical interaction data is still lacking. As physical touch is an important form of information transfer between humans and robots in shared environments and collaborative work, the ability to sense touch is important for improving human-robot collaboration [2].

The development of large area tactile sensing technologies for robots faces challenges such as the density of sensing elements, detection accuracy and cost. Traditional tactile sensors are based on physical transduction phenomena, while arrays formed of resistive sensors [3], capacitive sensors [4], ToF (time-of-flight) sensors [5], pressure sensors [6], magnetic sensors [7], etc. to detect or measure force/touch have been employed. These electronic methods require a large number of wires and analog-to-digital converters, which makes it difficult to improve the spatial resolution or provide large-area tactile sensing information for the robot. Miniaturizing the sensors also diminishes the initial sensor values making the sensitivity lower and the changes difficult to sense electronically [3]. Electrical impedance tomography (EIT) techniques that sense in a continuous resistive sheet suffer from low sensitivity in the regions sparsely populated with electrodes and require complicated instrumentation and computation [8]. Electronic sensors are also susceptible to environmental factors such as temperature changes, and interference from external magnetic fields limiting their application to industrial environments [9].

Introducing vision into tactile sensing tasks, by analyzing rich image information and converting it into tactile information, vision-based sensing achieves high spatial resolution with ease of manufacture and low cost, and can acquire the geometric or textural features of objects [10]. This also facilitates robots to have soft skins. The camera is placed inside the sensor, and the contact information on the sensor surface

This work was supported in part by UK EPSRC grant EP/T006951/1 and the Sussex Higher Education Innovation Fund, PhD Research Start-up Fund of Wuyi University (No. BSQD2222). *(Corresponding authors: Yanan Li and Hareesh Godaba)*

Lanhui Fu is with School of Intelligent Manufacturing, Wuyi University, Jiangmen 529020, China. Dip K. Saha, Shivraj Shere, Yanan Li, and Hareesh Godaba are with Department of Engineering and Informatics, University of Sussex, Brighton BN1 9RH, UK (e-mail: yl557@sussex.ac.uk, H.Godaba@sussex.ac.uk).

is separated from the camera, which makes the sensor more robust. Different types of cameras can be selected according to the size of the measurement area, and a large number of vision algorithms can be utilized to make the manufacture of vision-based tactile sensors more flexible and simple. In addition, camera-based sensing is easy to integrate into robotic control pipelines.

This study thus develops a soft tactile sensing based on vision to locate the touch points and estimate the force magnitude. The figure in abstract shows an operation scenario, in which this information of physical contact with the robot by a human hand is sensed and can be used to control the robot's movements. The main contributions of this work are as follows:

1) A new principle of vision-based sensing in which intensity modulation of light from flexible electroluminescent panels is used to realize a thin tactile sensing skin. This also enables replacing LEDs, avoiding the reflection effect of the enclosure wall. The EL panel is directly embedded inside the skin, and the skin area can be flexibly designed according to the application needs.

2) An image processing algorithm based on monocular vision using intensity as the detection index is developed to realize the localization of the contact point and the estimate the force magnitude.

This paper is structured as follows. Section II addresses the related works. Section III describes the fabrication process of the EL skin and the design of the whole system, followed by the detailed presentation of the vision-based model in section IV. A series of experiments for evaluation of the sensor performance are shown in section V. Finally, conclusions and future works are described in section VI.

II. Related works

Tactile sensors have, in the past, been embedded in robot fingertips, links of manipulators, arms and chest of humanoid robots, etc., to complete detection [3], grasping [11], environmental assessment [5] and other interactive tasks. Vision-based tactile sensors, which estimate contact information by visualizing the deformation of soft bodies/skin using cameras, are becoming popular because they offer high spatial resolution and rich contact information. They have attracted widespread attention in various robotic applications for contact detection, localization and force magnitude estimation [2].

A. Shape detection and force estimation in robotic fingertips

Some vision-based tactile sensors can acquire shape features of interacting objects which can then be used to perform subsequent grasping or classification tasks. The research on the localization and force magnitude is a further study on the basis of detection, which is of great significance in informing the action of the robot.

GelSight sensor [12] employed red, green and blue colors illuminating a clear surface. When there is a force applied, the surface deformation is recorded by a camera, visible dots are also marked on the surface to estimate the shape of the contact surface. Dong et al. [13] improved GelSight for 3D reconstruction of objects. Calandra et al. [14] imitated two human fingers by using two GelSight sensors to obtain grasping images, and built a neural network of tactile images and grasping states to predict grasping results. She et al. [15] proposed GelFlex based on GelSight, and designed two fingered grippers; each finger contains two fisheye cameras to detect the shape of objects and classify them. Patel et al. [16] mimicked human fingertips to find and classify objects in sand with improved GelSight. [17] presented a F-Touch sensor by adding an internal elastic structure on the basis of GelSight to realize estimation of three-axis force components, which was further extended to six-axis force/torque components [18] and shape recognition [19].

Tactip sensor [20] simulated the structure of the human fingertip, designed the silicone outer skin as a curved surface, and continuously reduced the size of the curved surface, to achieve object manipulation, contact sensing, pressure sensing and shear force detection. Winstone et al. [21] estimated force using two Tactip sensors. James et al. [22] distinguished sliding and stationary objects using Tactip and machine learning algorithms. Polic et al. [23] combined Tactip and CNN neural network to complete plant processing tasks such as pruning and picking.

GelSlim sensor [24] tuned the camera position to enlarge the illumination area, and improve the durability and contact signal strength of the gel. GelSlim focuses on shape and texture reconstruction of the contact objects, and it is usually used to finish peg-in-hole and dense packing tasks [25]. Ma [26] reconstructed the contact force distribution to propose a new version of the tactile sensor GelSlim 2.0.

In addition, other studies on shape detection and force estimation have been conducted. Shimonomura et al. [27] built a three-camera vision system in the grasping operation to calculate the distance and estimate the shape of the object through stereo matching. Ruijia et al. [28] applied particle image velocimetry to the field of vision-based tactile sensors for shape reconstruction and tracking. Vlack et al. [29] described GelForce, which uses vector distribution to calculate the force magnitude. Yamaguchi [30] designed a transparent finger vision system, which uses a camera for each finger to complete tasks such as contact force estimation. McInroe et al. [31] fabricated a haptically actuated, controllable stiffness device SOFTcell, to measure contact forces and moments. Referring to bionics, Kent et al. [32] provided a tactile sensor with a whisker array to discriminate inertial force, airflow, and contact force.

B. Vision-based tactile sensing for manipulator links

Tactile sensing for robot manipulator links is useful for obstacle detection and estimation in contact tasks as well as for human-robot interaction. The real-time estimation of the contact position and force magnitude is helpful for the robot to estimate the human intention [33], which is essential for many collaborative tasks. In contrast to robotic fingertips, manipulator links are large with curvatures making camera placement, lighting and image capture challenging. Although

some successful tactile sensors have been developed, there are significant limitations in localization and force magnitude estimation.

Isabella et al. [34] outlined a tactile sensor composed of a hemispherical film and a depth camera to correct and follow human finger movements. Zhang et al. [35] built a cylindrical tactile sensor similar to the human arm based on a fisheye lens, and used optical flow method to track markers on a soft substrate and detect the location of the applied force. Force estimation is challenging to achieve in that setup because the change in pixel position of markers in a thin skin is hard to accurately obtain. Yoshigi et al. [36] described a conical cylindrical sensor using two fisheye lenses to calculate the position and the depth of the sensor deformation based on the contact image.Duong et al. first promoted a sensing approach which could detect markers deflection [37], and then introduced TacLink [38] which used two cameras binocular vision to detect the changes in location of white markers in a black silicone pressurized structure to locate the point, and estimate the magnitude of the external force. However, it is challenging to achieve high spatial resolution and force sensitivity. As the silicone structure is a hollow shell, a force applied causes a large region of the shell to deform. This makes it challenging to obtain a high spatial resolution for multi-point detection. In addition, the internal pressure should be set to a low value (such as 0 or 0.5kPa) to achieve significant deformations in the structure to be captured by the camera. Under such internal pressure, the load bearing capability of the link is low and the force sensitivity decreases with increasing load-bearing capability. In addition, the soft link is pressurized and the force sensitivity varies across the length of the link. At the same time, tactile sensing based on stereo-camera has only been implemented for soft pressurized manipulators which do not have a rigid body and undergo significant deformations. On the basis of [38], [39] changed the skin to a polymer dispersed liquid crystal film, which can switch between the opaque and the transparent state, to collect tactile and proximity perception data in two modes. Luu et al. [40] proposed a pipeline named SimTacLS to analyze the dataset captured by the visual tactile sensor in the TacLink device in order to carry out tactile-driven robotics tasks. In these studies, the internal lighting system plays a crucial role in detecting the markers accurately. The material of the transparent parts should be selected or engineered carefully to remove any light reflections or other artifacts.

In our study, we develop a vision-based tactile sensor that uses a skin with its own light source to localize the contact position and estimate the force magnitude based on the intensity of light transmitted through a translucent layer. This sensor addresses the requirements of single point contact and multipoint contact estimation for human-robot interaction.

III. Design and Fabrication

A. ELTac sensing design

Fig.1 illustrates the detailed structure of the ELTac sensing module, which is a cylindrical sensor with the ability to detect multi-point touch on the cylindrical outer surface and

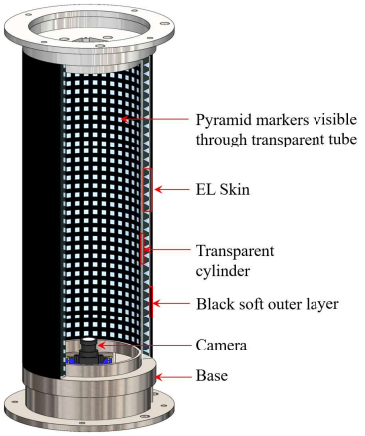

Fig. 1. Vision-based sensing with EL skin and one camera at the bottom.

estimate the magnitude of forces applied. The ELTac sensing module consists of a rigid transparent acrylic cylinder of outer diameter 80mm and inner diameter 76mm, mounted on a 3d-printed base that acts as a holder for the cylinder and can be used as a coupling to integrate with a robot arm. This acrylic cylinder acts as the skeleton of the sensor module and provides a rigid surface for the attachment of the electroluminescent skin. The holder houses a wide-angle USB camera (ELP_USBFHD04H_L21, ELP, China).

We develop soft deformable skin segments using off-the-shelf electroluminescent (EL) panels (EL Wire Craft, 70mm $\times$ 110mm, 0.31mm thickness, UK). EL panels are composed of two conductive layers, one of which is transparent to allow light transmission, sandwiching a semiconductor layer, that emits light when an alternating current is applied. These panels are flexible and can also be cut into desired shapes. EL panels are commercially available in many sizes (A6, A5, A4, A3, A2 and A1) and multiple colours. The thickness of a typical panel is about 300 μm. Each EL panel employed in the tactile sensing skin is powered by using only two electrical wires attached to the panel at one corner of the sheet and provides a large area for tactile sensing. Utilizing LEDs placed at different locations inside the tactile sensing module as a light source makes uniform illumination of the tactile sensing area difficult and sometimes causes interference due to reflection of LED light off the rigid surface supporting the elastomer skin. In contrast, embedding the EL panel inside the skin helps to achieve a uniform light environment throughout the tube. We use an inverter to convert 6.5V DC to 65V and 815Hz AC voltage and power the electroluminescent panel. We embed the EL panel inside silicone rubber, to form a soft skin (80mm $\times$ 120mm). Four segments of electroluminescent deformable EL skin are attached circumferentially onto the cylinder which act as the transducers that convert external force into a change in transmitted light intensity. The outer and top of the cylinder are covered with a thin layer of black elastomer to block external light from entering the sensor module. When an external force is applied to the ELTac surface, black soft skin and EL Skin are simultaneously pressed and the pyramidal structures on the

EL Skin deform due to pressure. The distance between the EL panel located inside the EL skin and the transparent acrylic tube at the point of force application becomes shorter, and the transmitted light intensity increases. The pixels corresponding to the deformed pyramids in the camera image get brighter. Finally, the magnitude of the applied force is calculated according to the experimentally mapped relationship between the fitted light intensity and force magnitude.

The difference from other works [35] [38] is threefold: first, in contrast to using the reflection of LED light by markers to detect marker locations, we use flexible EL panels as a light source and utilize the changes in the transmitted light intensity through a translucent medium. This removes the issue of reflection of LED light by the transparent acrylic tube and causing artifacts in the camera images. Second, although we use only a single camera in this study, this technique also allows one to safely use two cameras to improve spatial resolution without additional considerations about blocking light from being directly incident on the camera aperture. It not only saves the space of the light sources, but also simplifies the overall structure of the sensor, and the size and position of the electroluminescent sensing skin can be flexibly set according to the needs. Third, the force magnitude can be estimated directly from the intensity of the light transmitted from the specific point of interest and does not require two cameras and algorithms to compute deformations which can be computationally expensive. In this work, we use a single wide-angle USB camera, from which the light intensity of taxels is detected and the localization and force estimation are conducted. This is a localization method based on a monocular camera, which saves hardware costs and simplifies the computational complexity of image processing algorithms. To the best of our knowledge, this is the first application of electroluminescent skin to large area vision-based tactile sensing.

B. Fabrication of tactile skin based on EL panels

The EL skin is composed of four layers: the inner opaque black layer with apertures, a translucent middle layer, a flexible EL panel, and an opaque black outer layer (shown in Fig. 2). The middle translucent layer has pyramid shaped structures that project outward through the apertures in the inner opaque black layer. These structures act as stationary markers with variable brightness when viewed from the camera. The black inner layer has 8×12 holes, corresponding to 96 markers on the transparent middle layer. The EL panel is between the middle layer and the black bottom layer. We show the detailed process on how to prepare the EL skin in Fig. 3, which includes four steps.

1) Mold design. Three molds are designed, namely Mold 1, Mold 2 and Mold 3 in Fig. 4, and 3d printed with PLA material. The three molds are used to make three layers of silicone elastomer skin.

2) Black upper layer and black bottom layer. The upper layer is a black layer with holes, and the bottom layer is to cover the EL panel. Mix part A and part B of Silicone (Ecoflex0030, Smooth-On, Inc. USA) in a ratio of 1:1. Mix

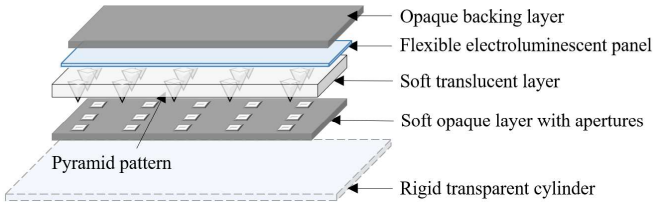

Fig. 2. The layers of EL skin.

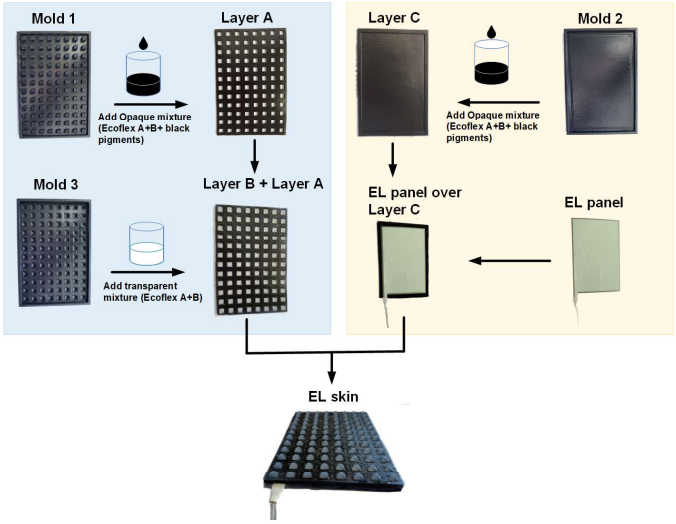

Fig. 3. The fabrication process of EL skin.

well after adding 1 drop of black paint, and use the vacuum pump to evacuate the air bubbles in the mixing. Pour into mold 1 and mold 2 and get skin 1 and skin 2 after four hours.

3) Transparent middle layer and markers. Place skin 1 inside mold 3 to make sure the holes are aligned. Then, mix Ecoflex0030 (15g part A+15g part B) without any color, after vacuuming, pour it into mold 3 where skin 1 is placed. After four hours, skin 3 with transparent pyramid markers and black gap is obtained, the size and the height of the pyramid is 6mm and 3mm, and the distance between the pyramids is 10mm. This design can avoid interference of edge intensity changes on the contact point.

4) Finally, place the EL panel on top of skin 2, and skin 3 on top of the EL panel. Use a small amount of mixed transparent silicone as glue and apply it between the three layers. After curing, the fabrication of the EL skin is completed.

The whole tactile sensor contains four EL skins and the entire cylindrical surface is then covered by a black soft skin, and the top of the tube is also covered by the black soft skin. The cylindrical structure with the EL skins is installed on a 3d printed base with a camera. This completes the fabrication of the ELTac, which is shown in Fig. 2.

IV. Vision-based model

A. Principle of vision-based model

The schematic diagram of the imaging system of the ELTac sensor is shown in Fig. 4. In the figure, the coordinates of a point on the sensor surface in the world coordinate

system are $M\left(X_M, Y_M, Z_M\right)$, the coordinates in the image coordinate system are $m\left(x_m, y_m\right)$, and the coordinates in the pixel coordinate system are (u, v). The distance between the focal point and the imaging plane is the focal length f. The distance between the focal point and the X-Y plane of the world coordinate system is d. We use cylindrical coordinates to represent the world coordinate system,

$$\begin{cases} X_M = R\cos\theta \\ Y_M = R\sin\theta \\ Z_M = Z_M \end{cases} \tag{1}$$

where R is the radius of the acrylic tube with a value of 40mm, and θ is the angle between the point M and the X axis. We use the polar coordinate system to represent the imaging coordinate system,

$$\begin{cases} x_m = r\cos\theta \\ y_m = r\sin\theta \end{cases} \tag{2}$$

where r is the distance from m to the origin of the imaging coordinate system. The axes of the image coordinate system are aligned with those of the world coordinate system, and the angle θ for a giving point in the world coordinate system is the same as that of its corresponding point in the image coordinate system. According to the principle of pinhole imaging, the relationship between point M in the world coordinate system and the imaging coordinate system can be obtained,

$$\frac{r}{R} = \frac{f}{d + Z_M} \tag{3}$$

Besides, the relationship between the imaging coordinate system and the pixel coordinate system is,

$$\begin{cases} x_m = u - c_x \\ y_m = v - c_y \end{cases} \tag{4}$$

where (c_x, c_y) is the coordinate of the principal point in the pixel coordinate system. After calculating the pixel coordinates of the contact point from the two-dimensional image, the coordinate of the imaging coordinate system can be obtained, and then r and θ can be calculated,

$$\begin{cases} r = \sqrt{x_m^2 + y_m^2} \\ \theta = \arctan 2\left(y_m, x_m\right) \end{cases} \tag{5}$$

f and d are obtained by calibration, and R is a known constant, so Z_M can be calculated according to (3), and then the coordinates of the point in the world coordinate system can be obtained using (1) to realize localization.

B. Model calibration

The transformation from the image plane to the world coordinate system is valid for a camera with a lens without distortion. However, most lenses have radial distortion. First, we calibrate the camera's internal parameters using Zhang's calibration method [41] and obtain the distortion parameters. The internal parameters are calculated by Camera Calibrator Toolbox in MATLAB as $f_x = 976.4, f_y = 976.6, c_x = 647.6, c_y = 357.5, k_1 = -0.4171, k_2 = 0.2501$. The images

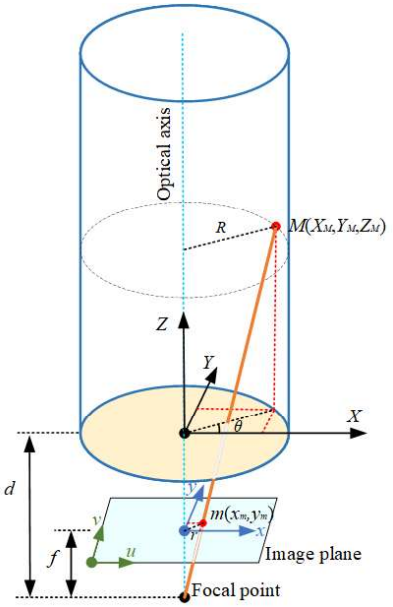

Fig. 4. The schematic diagram of the image system.

captured by the camera are then corrected according to the internal parameters using the following equation:

$$\begin{cases} x_m = \frac{\widetilde{x}_m}{1+k_1\widetilde{r}^2+k_2\widetilde{r}^4} \\ y_m = \frac{\widetilde{y}_m}{1+k_1\widetilde{r}^2+k_2\widetilde{r}^4} \end{cases} \tag{6}$$

where x_m and y_m are the corrected coordinates, $\widetilde{x}$ and $\widetilde{y}$ are the coordinates in the captured image, and $\widetilde{r}$ is the corresponding radial coordinate in the captured image. In order to obtain f and d in (3), we selected 15 points on the sensor inner surface, measured the Z_M value of each point, calculated the pixel coordinates of each point, and further obtained r by using (5) and (6). Since R is known, the optimal f and d can be calculated according to the least squares method, which are 784.7 and -38.21, respectively.

C. Force detection, localization and magnitude estimation

We developed methods for localizing either single point or multi-point contacts. In single point contact estimation, the location with maximum force application is localized while in multi-point contact localization, all the regions with force application are displayed. Fig. 5 shows the flow chart for the detection and localization of the contact point by the ELTac sensor.

First, we obtain a video frame and save it as the initial frame f_1. We subtract the subsequent frames from f_1 to obtain the frame difference df. As the color of the EL panel used in our work is light blue, we extract the Green and Blue components of df in the RGB color space and add them together to get the intensity value fr. At this time, it is necessary to determine whether single point detection or multipoint detection is required. For single point detection, we apply a smoothing filter to the image fr and find the maximum intensity and the corresponding pixel coordinate (u, v). The corresponding coordinate in the world coordinate system is

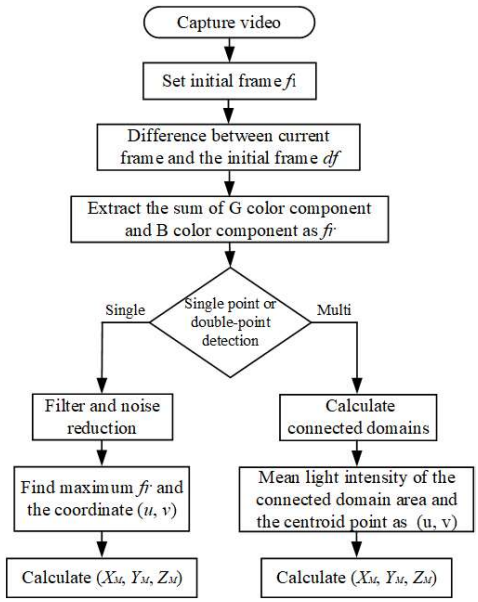

Fig. 5. Flow chart of the detection and localization of the touch points on sensor surface.

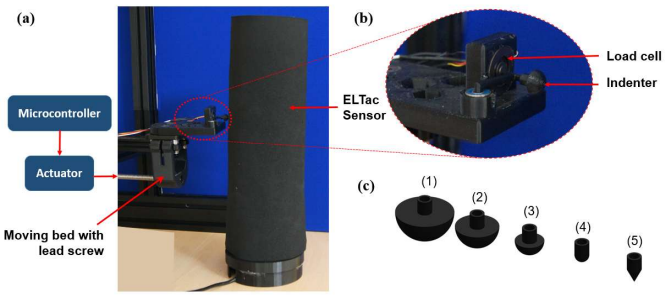

Fig. 6. Experiment platform, (a) load force sensor with indenter to measure the force magnitude, (b) enlarged view of the moving bed with load cell, and (c) five indenters with different radii.

then calculated according to the method in section IV.B. For multi-point detection, i.e., to display all the points with the force applied, we use the region growth algorithm to obtain the connected domain area in fr. When the connected domain area is larger than a threshold value P (400 in the experiment), the centroid point of this connected domain is considered to be the contact point, and the mean light intensity of the connected domain is calculated. Same as the single point detection, the corresponding coordinates of the barycentric points in the world coordinate system are then obtained according to the method in section IV.B.

V. Experiments and Results

A. Experiment setup

We assembled a test rig for experimental data collection as well as evaluation of sensor performance. A structure made of aluminum profiles is assembled to house a lead screw drive mounted horizontally. A load cell (FX29K0_100A_0010_L, TE Connectivity Sensors, US) with an indenter attached is mounted on the moving bed of the lead-screw drive to apply forces on the surface of the EL skin and record the force

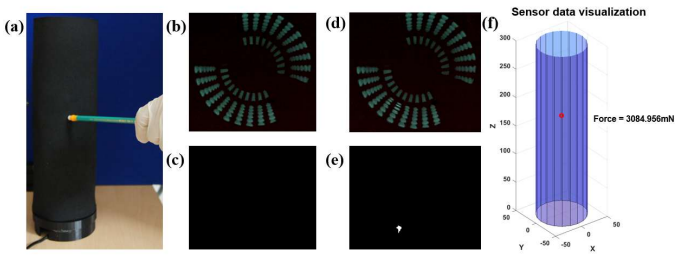

Fig. 7. Single point detection results, (a) experiment scenario, (b) original image, (c) original binary image, (d) pressed point in the captured image, (e) pressed point in the binary image, (f) sensor data visualization.

magnitude through a microcontroller (Arduino Uno Rev3, ELEGOO, China), as shown in Fig. 6(a). The lead-screw can be controlled using a RS PRO bipolar hybrid stepper motor and programmed using the microcontroller through a TB6600 stepper motor driver. The aluminum profile structure can be adjusted to place the lead-screw drive at different heights and positions to indent different locations on the sensor surface. Five types of indenters (Fig.6(b), a 5mm conical tip and hemispherical tips of diameters 5mm, 10mm, 15mm and 20mm) are set in front of the force sensor (Fig. 6(c)), to touch the ELTac sensor. We use MATLAB to implement the algorithm on a laptop with Intel (R) Core (TM) i7_9750H @2.6 GHz 2.59GHz, 16.0 GB RAM, NVIDIA GeForce RTX 2070 with Max-Q Design, to verify the performance of ELTac sensor.

B. Contact localization

When an external force is applied on the ELTac sensor, the intensity of the markers on the EL skin will increase. The position of the force on the captured image is obtained through the detection algorithm proposed in section IV C. Then, the coordinate values in the world coordinate system are visualized on the simulated ELTac sensor. Fig. 7 shows an example of single point contact force detection. When a concentrated force was applied on the surface of the sensor, the brightness of the corresponding markers increased and the brighter region was segmented based on the procedure in section IV.C (Fig. 7(b)). The barycenter of this connected region was transformed to the world coordinate system and was plotted on a mesh visualizing the sensor surface (Fig. 7(c)). Fig. 8 shows the results of multi-point force detection in which the force was applied at two different points on the surface simultaneously. The 3D positions of these two forces were displayed on the sensor geometry in Fig. 8(b).

In order to measure the accuracy of force localization and the robustness to the shape of the object applying the force, we tested the sensor with five different indenters at 12 arbitrarily chosen locations on the sensor surface in a total of 42 sets of data, and recorded the detected coordinate values (X_M, Y_M, Z_M) in the world coordinate system. At the same time, we manually measured the height $Z_{M\ \mathrm{truth}}$ of the contact point and the angle θ_{truth} between the point and the X axis, and calculate the real coordinate

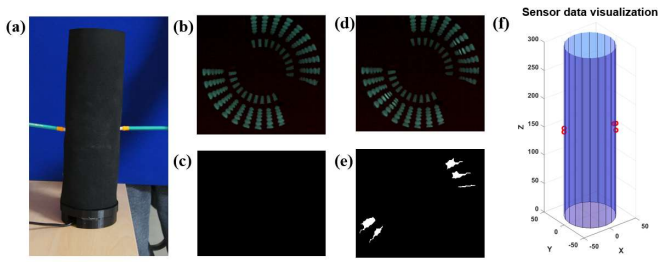

Fig. 8. Multipoint point detection results, (a) experiment scenario, (b) original image, (c) original binary image, (d) pressed point in the captured image, (e) pressed point in the binary image, (f) sensor data visualization.

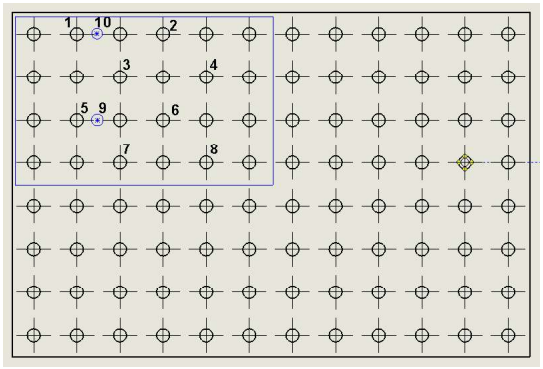

Fig. 10. Ten arbitrary data measuring points on the ELTAc surface.

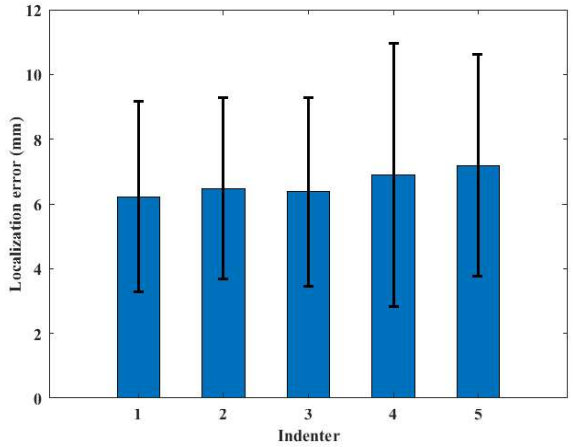

Fig. 9. Localization errors for the five indenters.

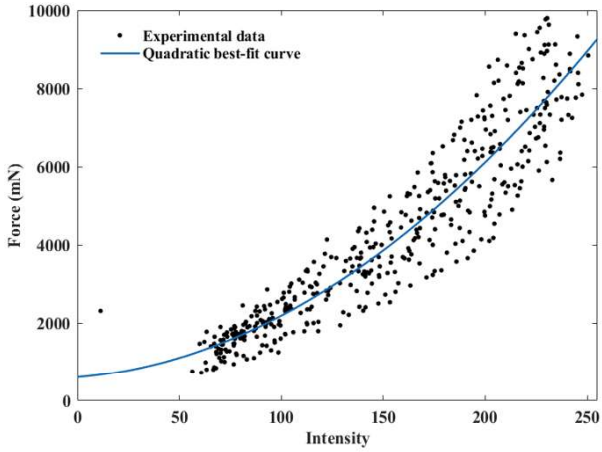

Fig. 11. Best-fit curve (Force vs Intensity).

$(X_{M\ \text{truth},}, Y_{M\ \text{truth}}, Z_{M\ \text{truth}})$. We then calculated the Euclidean distance between the detected coordinate and the real coordinate as the localization error, as shown in Fig. 9. Among the five indenters, the average localization error of indenter1 is the smallest (6.22mm), while the average localization error of indenter5 is the largest (7.19mm). The average localization error of indenter 2 to indenter 4 is 6.47mm, 6.37mm, 6.90mm, respectively. The average localization error is 6.63mm, which is comparable to the distance between consecutive pyramids in the EL skin which is 10mm. This points to a potential approach for improving the localization error by reducing the distance between the pyramids.

C. Force estimation

The best-fit curve for relationship between applied force and the marker intensity was generated from the complete dataset covering a wide range of force data using indenter2, indenter3, and indenter4 with numerous data measuring points. The characteristic of the force and intensity relation was represented by a quadratic equation $F(I) = p_1 I^2 + p_2 I + p_3$. For each measuring point, three different forces 3000mN, 5000mN, and 9000mN were applied to measure the corresponding intensity of the ELTAc sensor to cover the full range of the data set. Ten arbitrary measuring points, as shown in Fig. 10, were selected on the ELTAc surface to characterize the relation of pixel intensity to the force applied. Points 1-8 are directly on the top of the pyramid, whereas points 9-10 are between two pyramids. Indenter 3 with a tip radius of 10mm was considered to ensure consistency in the experiment. The force measured directly from the load cell was compared with the calculated one obtained from the best-fit curve, as shown in Fig. 11. The coefficients are $p_1 = 0.117, p_2 = 4.171, p_3 = 599.9$.

The comparative analysis between measured force and estimated force is shown in Table I. We use $E = 100(FL - Fc)/(FL)$ to calculate the absolute force estimation error. Here, FL and Fc are the measured force from the load cell and the estimated force, respectively. *F10* indicates the average value of the estimated force from the last ten image frame. *F5*, *F3*, and *F1* indicate the average values of the last five, three and one iterations, respectively. The average error obtained by the last three iterations (*E3*) is 9.3%, the smallest among all. The maximum error produced by the *E1*, which is 11.7%, is in an acceptable range. The average force estimation error is 10.45%. The standard deviation falls in 7.6 - 8.2% range, which also looks consistent in error generation. It is also observed that the force estimation is much more accurate in the central zone of the sensor than in the edge region, such as data points 1, 2, and 10. We expect that improving the attachment of the ELTAc sensor with the acrylic tube would improve the performance. Besides this, the ELTAc sensor was

TABLE I
FORCE ESTIMATION RESULTS

Data measuring points	Measured force *FL* (mN)	Estimated force from best-fit curve *Fc* (mN)				Absolute Force estimation error (%)			
		F10	F5	F3	F1	E10	E5	E3	E1
3	3053	2750	2646	2649	2445	9.9	13.3	13.2	19.9
	5270	5631	5568	5423	5616	6.8	5.6	2.9	6.6
	8001	7388	7541	7633	7807	7.7	5.7	4.6	2.4
4	3053	3040	3017	3095	3154	0.4	1.2	1.4	3.3
	5110	5013	5004	5036	4868	1.9	2.1	1.5	4.7
	8239	8053	8030	8024	7691	2.3	2.5	2.6	6.7
5	3092	2943	2893	2949	2850	4.8	6.4	4.6	7.8
	5007	4788	4850	4958	5471	4.4	3.1	1	9.3
	8021	7086	7225	7348	7865	11.7	9.9	8.4	1.9
6	3035	2339	2397	2514	2445	22.9	21	17.2	19.5
	5053	4512	4499	4529	4473	10.7	11	10.4	11.5
	8197	7604	7610	7749	7348	7.2	7.2	5.5	10.4
7	3067	3393	3470	3503	3440	10.6	13.1	14.2	12.2
	5170	5253	5207	5249	5423	1.6	0.7	1.5	4.9
	8178	7326	7416	7365	6796	10.4	9.3	9.9	16.9
8	3160	2454	2474	2587	2504	22.4	21.7	18.1	20.7
	5192	4371	4491	4376	4346	15.8	13.5	15.7	16.3
	8400	5942	5942	5947	5568	29.3	29.3	29.2	33.7
9	4100	3335	3514	3691	3589	18.7	14.3	10	12.5
	5110	4976	4895	4913	4734	2.6	4.2	3.9	7.4
	9367	7405	7576	7558	7749	20.9	19.1	19.3	17.3
			Average error			10.6	10.2	9.3	11.7
			Standard deviation			8.2	7.7	7.6	7.8

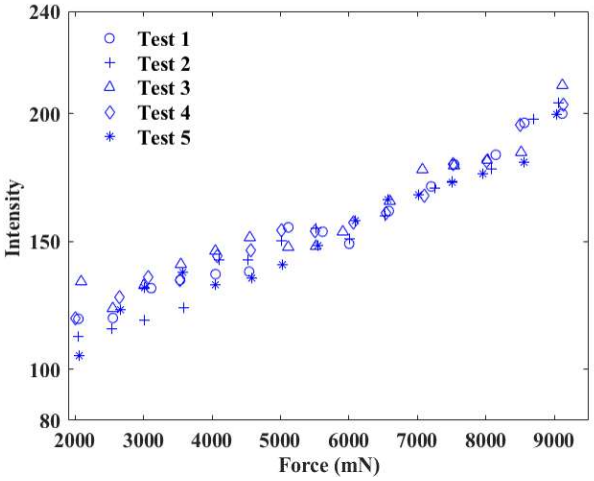

Fig. 12. Repeatability test (force vs intensity).

fabricated by combining several EL panels. Using a single large EL panel will also make the sensor more homogeneous and improve the overall force estimation accuracy further.

D. Repeatability and hysteresis test

A repeatability experiment was performed to investigate the robustness of the developed ELTAc sensor. The variation of pixel intensity to applied force was measured five times by indenting point 5 using indenter3. The interval between any two consecutive trials was at least one hour. A wide range of forces from 2000 to 9000mN were applied keeping other parameters constant. The force vs intensity data points for the five trials are shown in Fig. 12. We can find that the sensor has good repeatability.

As elastomer materials show time-dependent elastic behaviour, it is essential to calculate the hysteresis loss of the ELTAc sensor. Therefore, the same loading and unloading

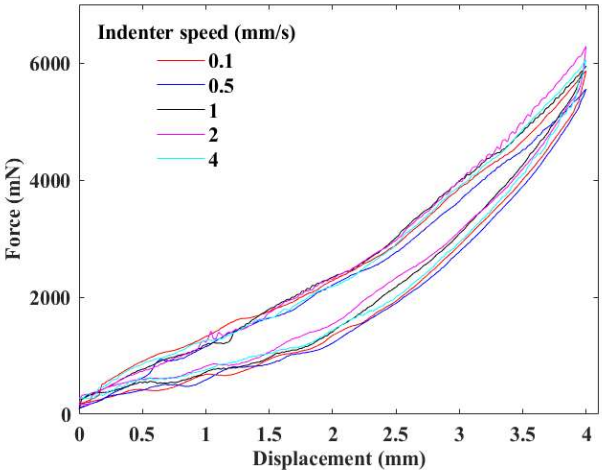

Fig. 13. Hysteresis test (force vs displacement).

TABLE II
ENERGY LOSS CALCULATION DUE TO HYSTERESIS

Indenter speed (mm/s)	0.1	0.5	1	2	4
Hysteresis loss (%)	28.27	25.68	23.27	21.62	23.84

cycle (0 to 4mm) was applied to the sensor at different indenter speeds to evaluate the hysteresis loss. Throughout the experiment, indenter3 was used to apply forces to measuring point 4 at different indenter speeds varying from 0.1mm/s to 4mm/s precisely controlled using a stepper motor driver. Fig. 13 shows the hysteresis loops for different indenter speeds. The sensor offers a certain amount of hysteresis as the response did not follow the same path during loading and unloading. However, the sensor's performance is consistent in terms of energy loss, as shown in Table II. The hysteresis losses for all the 5 speeds are within 30% with no significant differences within this speed range.

VI. DISCUSSION

To compare with other related works on vision-based large area tactile sensing, we summarize various methodology information and performance indicators in Table III - image capture, image resolution, light source, sensor function, localization error range and force estimation error range. As can be seen from the table, our work is the only one that does not use LEDs. Placement of LEDs is crucial to achieve uniform illumination and reduce interference caused due to reflection of light from internal surfaces of the sensing module. Our methodology based on embedding EL panels into the soft skin not only helps to achieve uniform illumination but also introduces attenuated light through the acrylic tube removing interference and need for complex image processing techniques. For image capture, two-camera systems and the triangulation principle for localization are typical in the large area tactile sensing studies. In this work, the force at a point is directly related to the intensity of the corresponding pixels in the image removing the need for marker tracking in a 3d coordinate system that requires two cameras. The localization error in our work is 6.22–7.19mm. This range is comparable

TABLE III
COMPARISON WITH OTHER WORKS

Reference	Image capture	Image resolution	Light source	Sensor function	Localization error range	Force estimation error range
Duong [37]	Two fish-eye cameras	640×480	LEDs	Detect each marker's deflection	–	–
Yoshigi [36]	Two fish-eye cameras	360×360	LEDs	Detect the localization area	Detection accuracy (94.55% to 98.18%)	–
Duong [38]	Two fish-eye cameras	640×480	LEDs	Localization and force estimation	Mesh size of 18mm × 9.5mm	Below 0.7mm depth error
Luu [39]	Two fish-eye cameras	640×480	LEDs	Contact depth estimation	–	1.22mm depth error at 5mm's contact depth case
Luu [40]	Two fish-eye cameras	640×480	–	Contact detection and localization	4.86-7.19mm	–
Zhang [35]	One fish-eye camera	1640×1232	LEDs	Localization and mimic human actions	–	–
This work	One wide-angle camera	1280×720	EL Panels	Localization and force estimation	6.22-7.19mm	9.3-11.7%

to that in Luu et al. [40] and to the mesh size of 18mm × 9.5mm employed for localization in Duong et al. [38] . To the best of our knowledge, very few studies in literature focused on force estimation in large area tactile sensing. In [38], a finite element model (FEM) method was developed to convert marker displacements obtained by image processing into force estimation in a soft internally pressurized structure. When the internal pressure is 0 kPa, the predicted results are very close to the ground truth with the absolute errors corresponding to 5% full scale. As the internal pressure increases, the force estimation error also increases with the absolute error reaching about 70%. In comparison, our approach does not have such interdependence, and the error range of force estimation is smaller at 9.3-11.7%. To the best of our knowledge, there is no shear force estimation in large area tactile sensing modules. The methodology in this paper is limited to normal force estimation and is not suitable for shear force sensing. In contrast, the other methodologies based on marker tracking [35-40], in principle, allow for complete mapping of the deformation field and hence the potential for directional and shear forces. In summary, the ELTac sensing module offers high localization and force estimation accuracies as well as multi-point contact detection capabilities all enabled by a single camera.

VII. CONCLUSION

In this paper, we designed a novel vision-based tactile sensor ELTac, by using one camera, to realize contact localization and force magnitude information. We use EL panels that can be freely selected in shape and can be cut arbitrarily instead of LEDs to provide the light source, which avoids the problem of reflection off the inner transparent tube surfaces. A localization method based on a monocular camera is presented. By obtaining the intensity change between different frames and calculating the contact position, the minimum average localization error of the five indenters is 6.63mm. The detection algorithm realizes single point contact force detection and multi-point detection, which could be used for various human-robot interaction applications. Finally, the intensity-force mapping relationship at different positions on the sensor surface is analyzed. The average error of force detection falls in 9.3-11.7% range. Repeatability and hysteresis tests show that the ELTac skin can be a reliable and promising candidate for large area tactile sensing. In our future work, we will focus on monolithic EL skin fabrication for continuous large area coverage and improved homogeneity, as well as methods to improve the sensor's spatial resolution. We will also explore integration of the sensor with robotic manipulators for human-robot collaborative tasks.

REFERENCES

[1] F. Mohammadi Amin, M. Rezayati, H. W. van de Venn, and H. Karimpour, "A mixed-perception approach for safe human–robot collaboration in industrial automation," *Sensors*, vol. 20, no. 21, p. 6347, 2020.

[2] Q. Li, O. Kroemer, Z. Su, F. F. Veiga, M. Kaboli, and H. J. Ritter, "A review of tactile information: Perception and action through touch," *IEEE Transactions on Robotics*, vol. 36, no. 6, pp. 1619–1634, 2020.

[3] A. Schmitz, P. Maiolino, M. Maggiali, L. Natale, G. Cannata, and G. Metta, "Methods and technologies for the implementation of large-scale robot tactile sensors," *IEEE Transactions on Robotics*, vol. 27, no. 3, pp. 389–400, 2011.

[4] K. Park, H. Park, H. Lee, S. Park, and J. Kim, "An ERT-based robotic skin with sparsely distributed electrodes: Structure, fabrication, and DNN-based signal processing," in *2020 IEEE International Conference on Robotics and Automation (ICRA)*. IEEE, 2020, pp. 1617–1624.

[5] S. Tsuji and T. Kohama, "Proximity skin sensor using time-of-flight sensor for human collaborative robot," *IEEE Sensors Journal*, vol. 19, no. 14, pp. 5859–5864, 2019.

[6] A. Albini, S. Denei, and G. Cannata, "Human hand recognition from robotic skin measurements in human-robot physical interactions," in *2017 IEEE/RSJ International Conference on Intelligent Robots and Systems (IROS)*. IEEE, 2017, pp. 4348–4353.

[7] T. P. Tomo, A. Schmitz, W. K. Wong, H. Kristanto, S. Somlor, J. Hwang, L. Jamone, and S. Sugano, "Covering a robot fingertip with uskin: A soft electronic skin with distributed 3-axis force sensitive elements for robot hands," *IEEE Robotics and Automation Letters*, vol. 3, no. 1, pp. 124–131, 2017.

[8] A. B. Dawood, H. Godaba, A. Ataka, and K. Althoefer, "Silicone-based capacitive e-skin for exteroception and proprioception," in *2020 IEEE/RSJ International Conference on Intelligent Robots and Systems (IROS)*. IEEE, 2020, pp. 8951–8956.

[9] H. Wang, M. Totaro, and L. Beccai, "Toward perceptive soft robots: Progress and challenges," *Advanced Science*, vol. 5, no. 9, p. 1800541, 2018.

[10] K. Shimonomura, "Tactile image sensors employing camera: A review," *Sensors*, vol. 19, no. 18, p. 3933, 2019.

[11] R. Li, R. Platt, W. Yuan, A. ten Pas, N. Roscup, M. A. Srinivasan, and E. Adelson, "Localization and manipulation of small parts using gelsight tactile sensing," in *2014 IEEE/RSJ International Conference on Intelligent Robots and Systems*. IEEE, 2014, pp. 3988–3993.

[12] M. K. Johnson and E. H. Adelson, "Retrographic sensing for the measurement of surface texture and shape," in *2009 IEEE Conference on Computer Vision and Pattern Recognition*. IEEE, 2009, pp. 1070–1077.

[13] S. Dong, W. Yuan, and E. H. Adelson, "Improved gelsight tactile sensor for measuring geometry and slip," in *2017 IEEE/RSJ International Conference on Intelligent Robots and Systems (IROS)*. IEEE, 2017, pp. 137–144.

[14] R. Calandra, A. Owens, D. Jayaraman, J. Lin, W. Yuan, J. Malik, E. H. Adelson, and S. Levine, "More than a feeling: Learning to grasp and regrasp using vision and touch," *IEEE Robotics and Automation Letters*, vol. 3, no. 4, pp. 3300–3307, 2018.

[15] Y. She, S. Q. Liu, P. Yu, and E. Adelson, "Exoskeleton-covered soft finger with vision-based proprioception and tactile sensing," in *2020 IEEE International Conference on Robotics and Automation (ICRA)*. IEEE, 2020, pp. 10 075–10 081.

[16] R. Patel, R. Ouyang, B. Romero, and E. Adelson, "Digger finger: Gelsight tactile sensor for object identification inside granular media," in *Experimental Robotics: The 17th International Symposium*. Springer, 2021, pp. 105–115.

[17] W. Li, Y. Noh, A. Alomainy, I. Vitanov, Y. Zheng, P. Qi, and K. Althoefer, "F-touch sensor for three-axis forces measurement and geometry observation," in *2020 IEEE SENSORS*. IEEE, 2020, pp. 1–4.

[18] W. Li, A. Alomainy, I. Vitanov, Y. Noh, P. Qi, and K. Althoefer, "F-touch sensor: Concurrent geometry perception and multi-axis force measurement," *IEEE Sensors Journal*, vol. 21, no. 4, pp. 4300–4309, 2020.

[19] X. Li, W. Li, Y. Zheng, K. Althoefer, and P. Qi, "Criminisi algorithm applied to a gelsight fingertip sensor for multi-modality perception," in *2020 IEEE/ASME International Conference on Advanced Intelligent Mechatronics (AIM)*. IEEE, 2020, pp. 190–195.

[20] C. Chorley, C. Melhuish, T. Pipe, and J. Rossiter, "Development of a tactile sensor based on biologically inspired edge encoding," in *2009 International Conference on Advanced Robotics*. IEEE, 2009, pp. 1–6.

[21] B. Winstone, G. Griffiths, C. Melhuish, T. Pipe, and J. Rossiter, "Tactip—tactile fingertip device, challenges in reduction of size to ready for robot hand integration," in *2012 IEEE International Conference on Robotics and Biomimetics (ROBIO)*. IEEE, 2012, pp. 160–166.

[22] J. W. James, N. Pestell, and N. F. Lepora, "Slip detection with a biomimetic tactile sensor," *IEEE Robotics and Automation Letters*, vol. 3, no. 4, pp. 3340–3346, 2018.

[23] M. Polic, I. Krajacic, N. Lepora, and M. Orsag, "Convolutional autoencoder for feature extraction in tactile sensing," *IEEE Robotics and Automation Letters*, vol. 4, no. 4, pp. 3671–3678, 2019.

[24] E. Donlon, S. Dong, M. Liu, J. Li, E. Adelson, and A. Rodriguez, "Gelslim: A high-resolution, compact, robust, and calibrated tactile-sensing finger," in *2018 IEEE/RSJ International Conference on Intelligent Robots and Systems (IROS)*. IEEE, 2018, pp. 1927–1934.

[25] S. Dong and A. Rodriguez, "Tactile-based insertion for dense box-packing," in *2019 IEEE/RSJ International Conference on Intelligent Robots and Systems (IROS)*. IEEE, 2019, pp. 7953–7960.

[26] D. Ma, E. Donlon, S. Dong, and A. Rodriguez, "Dense tactile force estimation using gelslim and inverse fem," in *2019 International Conference on Robotics and Automation (ICRA)*, 2019, pp. 5418–5424.

[27] K. Shimonomura, H. Nakashima, and K. Nozu, "Robotic grasp control with high-resolution combined tactile and proximity sensing," in *2016 IEEE International Conference on Robotics and automation (ICRA)*. IEEE, 2016, pp. 138–143.

[28] R. Wang, C. Jiang, B. Yang, and J. Liu, "A novel vision-based tactile sensor using particle image velocimetry for multi-modal object detection and force sensing," in *2021 IEEE 34th International Conference on Micro Electro Mechanical Systems (MEMS)*. IEEE, 2021, pp. 764–767.

[29] K. Vlack, K. Kamiyama, T. Mizota, H. Kajimoto, N. Kawakami, and S. Tachi, "Gelforce: A traction field tactile sensor for rich human-computer interaction," in *IEEE Conference on Robotics and Automation, 2004. TExCRA Technical Exhibition Based.* IEEE, 2004, pp. 11–12.

[30] A. Yamaguchi and C. G. Atkeson, "Combining finger vision and optical tactile sensing: Reducing and handling errors while cutting vegetables," in *2016 IEEE-RAS 16th International Conference on Humanoid Robots (Humanoids)*. IEEE, 2016, pp. 1045–1051.

[31] B. W. McInroe, C. L. Chen, K. Y. Goldberg, R. Bajcsy, and R. S. Fearing, "Towards a soft fingertip with integrated sensing and actuation," in *2018 IEEE/RSJ International Conference on Intelligent Robots and Systems (IROS)*. IEEE, 2018, pp. 6437–6444.

[32] T. A. Kent, S. Kim, G. Kornilowicz, W. Yuan, M. J. Hartmann, and S. Bergbreiter, "Whisksight: A reconfigurable, vision-based, optical whisker sensing array for simultaneous contact, airflow, and inertia stimulus detection," *IEEE Robotics and Automation Letters*, vol. 6, no. 2, pp. 3357–3364, 2021.

[33] Y. Li and S. S. Ge, "Human–robot collaboration based on motion intention estimation," *IEEE/ASME Transactions on Mechatronics*, vol. 19, no. 3, pp. 1007–1014, 2013.

[34] I. Huang and R. Bajcsy, "High resolution soft tactile interface for physical human-robot interaction," in *2020 IEEE International Conference on Robotics and Automation (ICRA)*. IEEE, 2020, pp. 1705–1711.

[35] Y. Zhang, G. Zhang, Y. Du, and M. Y. Wang, "Vtacarm: A vision-based tactile sensing augmented robotic arm with application to human-robot interaction," in *2020 IEEE 16th International Conference on Automation Science and Engineering (CASE)*. IEEE, 2020, pp. 35–42.

[36] S. Yoshigi, J. Wang, S. Nakayama *et al.*, "Deep learning-based whole-arm soft tactile sensation," in *2020 3rd IEEE International Conference on Soft Robotics (RoboSoft)*. IEEE, 2020, pp. 132–137.

[37] L. Van Duong, R. Asahina, J. Wang *et al.*, "Development of a vision-based soft tactile muscularis," in *2019 2nd IEEE International Conference on Soft Robotics (RoboSoft)*. IEEE, 2019, pp. 343–348.

[38] L. Van Duong and V. A. Ho, "Large-scale vision-based tactile sensing for robot links: Design, modeling, and evaluation," *IEEE Transactions on Robotics*, vol. 37, no. 2, pp. 390–403, 2021.

[39] Q. K. Luu, D. Q. Nguyen, N. H. Nguyen *et al.*, "Soft robotic link with controllable transparency for vision-based tactile and proximity sensing," in *2023 IEEE International Conference on Soft Robotics (RoboSoft)*. IEEE, 2023, pp. 1–6.

[40] Q. K. Luu, N. H. Nguyen *et al.*, "Simulation, learning, and application of vision-based tactile sensing at large scale," *IEEE Transactions on Robotics*, vol. 39, no. 3, pp. 2003–2019, 2023.

[41] Z. Zhang, "A flexible new technique for camera calibration," *IEEE Transactions on Pattern Analysis and Machine Intelligence*, vol. 22, no. 11, pp. 1330–1334, 2000.

Lanhui Fu received the B.S. degree from Zhengzhou University, China, in 2009, the M.S. degree from Harbin Institute of Technology, China, in 2012, and the Ph.D. degree from South China Agricultural University, China, in 2022. She is currently a lecturer in Faculty of Manufacturing, Wuyi University, Guangdong, China. From 2021 to 2022, she was an academic visitor with the Department of Engineering and Design, University of Sussex, U.K. Her research interests include image processing, tactile sensing, machine vision and deep learning.

Dip Kumar Saha is currently pursuing his PhD in Engineering at the University of Sussex. He received his B.Sc. and M.Sc. in Mechanical Engineering from Rajshahi University of Engineering Technology (RUET), Bangladesh. His research interests include but are not limited to the sensorization of soft robotics, tactile sensing, and machine learning.

Shivraj Shere received a bachelor's degree (B.E.) in mechanical engineering from the Shivaji University, India in 2019 and an M.Sc. in Robotics and Autonomous Systems from the University of Sussex, UK in 2022. He is currently working as a robotics engineer at Ivy Tech with a focus on developing sustainable robotics solutions for the industry.

Yanan Li (M14-SM21) received the B.Eng. and M.Eng. degrees from the Harbin Institute of Technology, China, in 2006 and 2008, respectively, and the Ph.D. degree from the National University of Singapore, Singapore, in 2013. He is currently a Reader in Robotics with the Department of Engineering and Design, University of Sussex, U.K. From 2015 to 2017, he was a Research Associate with the Department of Bioengineering, Imperial College London, London, U.K. From 2013 to 2015, he was a Research Scientist with the Institute for Infocomm Research, Agency for Science, Technology and Research, Singapore. His general research interests include human-robot interaction, robot control and control theory and applications.

Hareesh Godaba received the B.Tech.(Hons.) degree from the Indian Institute of Technology (IIT) Bhubaneswar, Bhubaneswar, India, in 2013, and the Ph.D. degree from the National University of Singapore (NUS), Singapore, in 2018, both in mechanical engineering. He is currently a Lecturer in Engineering with the Department of Engineering and Design, University of Sussex, U.K. From 2018-2020, he had been a postdoctoral research associate at the Queen Mary University of London. His primary research interests include soft robotics, electroactive technologies, and tactile sensing.